CERTIFICATE OF MAILING

I hereby certify that this correspondence is being deposited with the United States Postal Service as first class mail in an envelope addressed to: Commissioner of Patents and Trademarks, Washington, D.C. 20231, on January 5, 2004.

Attorney for Applicant

PATENT
Docket No. SJ0920010058US1

IN THE UNITED STATES PATENT AND TRADEMARK OFFICE

Applicant:	Tsann Lin, et al.	
Serial No.:	10/066,835	
Filed:	February 4, 2002	Group Art Unit: 1773
For:	*IN-SITU* OXIDIZED FILMS FOR USE AS GAP LAYERS FOR A SPIN-VALVE SENSOR AND METHODS OF MANUFACTURE	
Examiner:	Kevin M. Bernatz	

DECLARATION UNDER 37 C.F.R. §1.132

Commissioner for Patents
P.O. Box 1450
Alexandria, VA 22313-1450
Dear Sir:

I, Tsann Lin, declare as follows:

1. I am an employee of Hitachi Global Storage Technologies, Inc. (Hitachi).

2. I am a former employee of a department of IBM which has been sold to Hitachi.

3. I am familiar with the contents and subject matter of the above-identified patent application having Serial Number 10/066,835 now owned by Hitachi.

4. I am a co-inventor with Daniele Mauri of the invention which is the subject of the above-identified patent application.

5. It is my understanding that United States Patent Application Publication number 09/748,207 by Sasaki et al. (hereinafter "Sasaki") has been cited as a primary reference in an Office Action by the U.S. Patent and Trademark Office.

6. I assert that the gap layer of the above-identified patent application is formed by a process of forming successive *in-situ* oxidized metallic layers. Pure Al is deposited using Physical Vapor Deposition (PVD). The thin layer of Al is substantially devoid of contaminants because the layer is deposited in a high vacuum. Oxygen is then introduced and the thin layer of Al is then *in-situ* oxidized such that full oxidation occurs. Full oxidation is possible because the metal layer is so thin. The gap layer serves as an insulation layer between a Giant Magneto Resistance (GMR) sensor and a shield layer or on either end of a Tunneling Magneto Resistance (TMR) sensor. Full oxidation provides an optimal insulation layer. Full oxidation also provides a gap layer having resistance properties superior to metal oxide layers formed using Chemical Vapor Deposition (CVD), as in Sasaki. I assert that the purity of the metal film and full oxidation of the metal contribute to the film comprising a negligible number of undesirable non-oxidized AL or other metal atoms.

7. I assert that in contrast, Sasaki teaches metal oxide films that are physically very different. In Sasaki, metal oxide films are formed using Low Pressure Chemical Vapor Deposition (LPCVD or CVD). LPCVD involves forming of an aluminum oxide, by a chemical reaction between two gases that are intermittently injected where one gas may be H_2O, N_2O or H_2O_2; the other may be $Al(CH_3)_3$ or Al_2Cl_3. Due to the chemical deposition, full oxidation of a gap layer using the CVD process is extremely difficult. Although a CVD process may be used to produce a 10 angstrom gap layer, the insulation properties are not sufficient. Consequently, in order to prevent shunting, the thickness of the gap layer taught by Sasaki, is ten times thicker than that of the claimed invention. The larger gap layer thickness restricts the use of the GMR sensor for ultrahigh-density magnetic recording.

8. I assert that there are three well known techniques for forming of metal oxides. Unfortunately, none of these methods produce a gap layer having electrical resistance as high as with *in-situ* oxidation of a pure, thin metal layer as in the claimed invention. The three methods of forming metal oxide films such as Al_2O_3 films are:

1. Direct Physical Vapor Deposition (PVD) sputter-deposition from an Al_2O_3 target;
2. Reactive PVD sputter-deposition in oxygen gas from an Al target; and

3. Chemical Vapor Deposition (CVD) where two gases are combined, one gas may be H_2O, N_2O or H_2O_2, the other may be $Al(CH_3)_3$ or Al_2Cl_3 the resulting Al_2O_3 is deposited onto a substrate;

These three methods share the same difficulty in achieving full oxidation. In other words, stoichiometric Al_2O_3 cannot be attained, thus leaving unwanted, non-oxidized Al or other metal atoms. As a result, the metal oxide films formed with these three methods will not provide the very high resistance needed for very thin gap layers used for ultrahigh-density magnetic recording. The degree to which the metal is oxidized according to the present invention, or any of the above methods is extremely difficult to quantify. However, the degree of oxidation may be derived by understanding the physical characteristics of the metal oxide that results. In method 1, the quality of the gap layer depends on the purity of the Al_2O_3 target. It is difficult to attain a good-quality gap layer since only a low-purity Al_2O_3 target can be fabricated with low-vacuum sintering of low-purity oxide powders. In method 2, the quality of the gap layer depends on the purity of the Al target and the oxygen doping extent during the reactive sputtering. In spite of the fact that a high-purity Al target can be fabricated with high-vacuum casting of a high-purity Al melt phase, it is still difficult to attain a good-quality gap layer since the oxygen doping extent cannot be as high as desired. At such a high oxygen doping extent, no oxide can be deposited since the deposition rate is nearly zero. In method 3, the quality of the gap layer depends on the purity of the gases at an early stage of the CVD process. It is difficult to attain a good-quality gap layer since unwanted Al, H_2O, N_2, H_2, C or Cl_2 may also be introduced into the oxide layer, and stoichiometric Al_2O_3 cannot be absorbed on a dissimilar surface in the early stage. In the present invention, the quality of the gap layer depends on the purity of the Al target and the *in situ* oxidation extent after the deposition of a very thin Al film. It is feasible to attain a high-quality gap layer since a high-purity Al target can be fabricated with high-vacuum casting of a high-purity Al melt phase, and the *in-situ* oxidation extent can be as high as desired. The very thin Al film with a closely packed face-centered-cubic crystalline lattice is first formed. Oxygen atoms are then introduced to fill vacancy sites of the crystalline lattice, and chemically bond to all the Al atoms for full oxidation. It should be noted that excessive oxygen gases can be introduced to ensure that full oxidation is attained.

In addition, the degree of oxidation may be derived by analyzing the physical characteristics of such layers when used in applications other than as a gap layer which requires the layer to be an optimal insulator (very high electrical resistance). For example, attempts have been made to use metal oxides for the barrier layer in a TMR (Tunneling Magnetoresistance) sensor. In order for a TMR sensor to work, there must be tunneling effects. To produce tunneling effects, there must be substantially no current flow through the barrier layer and there must be no metal elements in the barrier layer. Only a pure metal oxide will provide for no metal elements and no current flow (very high electrical resistance) such that conduction electrons will be forced to travel only by making quantun jumps ("the tunneling effect").

Attempts to use a barrier layer made of metallic oxide such as Al_2O_3 formed using the CVD process have been made and are explained in the paper entitled "ALCVD AlOx Barrier Layers for Magnetic Tunnel Junction Applications" (referred to herein as "ALCVD paper") by R. Bubber, M. Mao, T. Schneider, H. Hegde, K. Sin, S. Fundada, and S. Shi submitted herewith as exhibit A. This paper indicates that Al_2O_3 metallic oxide formed using CVD as taught by Sasaki fails to provide the high electrical resistance necessary to allow for the tunneling effect. *See* ALCVD paper page 3, left column, first line of first full paragraph, "The low junction resistance and the ohmic *I-V* feature indicate that the corresponding AlO_X x barrier layers are Al-rich, deviating from the stoichiometric Al_2O_3." In fact, Al_2O_3 metallic oxide formed with the three prior-art methods all fail to provide the high electrical resistance necessary to allow for the tunneling effect.

In contrast, a barrier layer formed using a metallic oxide formed using *in-situ* oxidation has been shown to prevent current flow across the layer and substantially eliminate metal elements such that tunneling effects are achieved. The paper entitled "A Tunneling Magnetoresistance Sensor Overlaid with a Longitudinal Bias Stack" (referred to herein as "Tunneling paper") by Tsann Lin, Daniele Mauri, and Philip M. Rice submitted herewith as exhibit B demonstrates this. Specifically, the barrier layer is made of Al-O and formed by *in-situ* oxidation. *See* Tunneling paper page 346, end of first paragraph and page 347, second sentence, top of right column. The paper demonstrates that a tunneling effect is achieved using a barrier layer of metallic oxide formed by *in-situ* oxidation.

Therefore, because a metal oxide formed using the CVD process as taught in Sasaki fails to allow for tunneling effects when used as a barrier layer in a TMR sensor and metallic oxides formed using the *in-situ* process allow for tunneling effects when used as the same layer, we can derive an understanding of differences between a metal oxide layer formed using the CVD process and one formed using *in-situ* oxidation. I assert that because tunneling effects require substantially no metal elements and no current flow, it is clear that the *in-situ* oxidized metallic layer has a higher resistance than a CVD metal oxide. Similarly, metal oxides formed using methods 1 and 2 above also fail to allow a tunneling effect. Consequently, the *in-situ* oxidized metallic layer is physically different and a superior insulator over metal oxides formed using conventional methods.

9. I assert that it is important to understand that during the deposition phase, the thickness of the metal is controlled so that the metal remains thin enough for the oxygen to fully chemically bond the metal. For example, the metal may be sputtered to no more than about ten Angstroms. *See* Specification page 14, line 13. Of course higher pressure and time of exposure to oxygen may be used to attain higher oxygen density in the metallic film.

10. I assert that the metal oxide films taught by Sasaki necessarily contain contaminants such as N, Al, or Cl. Such contaminates can cause the gap layer to short.

11. I declare further that all statements made herein of my own knowledge are true and that all statements made on information and belief are believed to be true; and further that these statements were made with the knowledge that willful, false statements and the like so made are punishable by fine or imprisonment, or both, under Section 1001 of Title 18 of the United States Code, and that such willful, false statements may jeopardize the validity of the application or any patent issuing thereon.

Dated this 31 day of December in the year 2003.

Tsann Lin

Tsann Lin

Exhibit A

ALCVD AlO_X Barrier Layers for Magnetic Tunnel Junction Applications

R. Bubber, M. Mao, T. Schneider, H. Hegde, K. Sin, S. Funada, and S. Shi

***Abstract*—Ultrathin AlO_x layers 5–25 Å thick were deposited using the atomic-layer chemical vapor deposition technique. A magnetic thickness loss of ~1 Å has been estimated at CoFe–AlO_x or NiFe–AlONiFe–AlO_x interfaces. The two-dimensional integrity of the thin AlO_x films at thickness >7 Å has been validated by the differential switching of two magnetic layers sandwiching a ultrathin AlO_x layer and the distinct cross-sectional transmission-electron-microscopy images. No appreciable tunnel magnetoresistance effect has been measured from the fabricated magnetic tunnel junction devices. A proper *in situ* treatment *prior to* and/or *after* AlO_x deposition and a proper protection of the underlying magnetic layer are expected for further improvements.**

***Index Terms*—Atomic-layer chemical vapor deposition (ALCVD), AlO_x, decoupling, J–V, magnetic thickness loss, magnetic tunnel junction (MTJ), thin films, tunnel magnetoresistance, tunnel barrier.**

I. Introduction

THE SELF-LIMITING growth nature of the atomic-layer chemical vapor deposition (ALCVD) technique [1], [2] allows depositions of very thin dielectric films with excellent conformality, uniformity, and atomic-level thickness control. It exhibits great potential for applications in magnetic recording heads and magnetic random-access memory, such as deposition of a thin oxide gap and a tunnel barrier layer. The challenge in implementing this technology lies in the control of surface chemistry and process conditions that are not necessarily compatible to the processing of magnetic materials and may, therefore, cause degradation in magnetic properties and device performance. In this paper, we evaluate the feasibility of ultrathin ALCVD AlO_x films as the tunnel barrier for magnetic tunnel junction (MTJ) applications.

II. Experimental Methods

Thin AlO_x films 7–100 Å thick were deposited using a CVD reactor [2]. A dual-zone injection mechanism was built in the CVD reactor for independent delivery of the reactants. The ALCVD deposition was realized by sequentially pulsing and inert gas purging of Trimethyl–aluminum (TMA), $(CH_3)_3Al$, and H_2O, which were delivered as gas pulses. The growth of thin AlO_x films was controlled in terms of process cycles with a deposition rate of typically 1 Å/cycle at 200 °C.

Manuscript received February 21, 2002; revised May 15, 2002.

R. Bubber, M. Mao, T. Schneider, and H. Hegde are with Fremont Application Lab of Veeco Instruments, Inc., Fremont, CA 94538 USA (e-mail: mmao@veeco.com).

K. Sin, S. Funada, and S. Shi are with Read-Rite Corporation, Fremont, CA 94539 USA.

Digital Object Identifier 10.1109/TMAG.2002.803163.

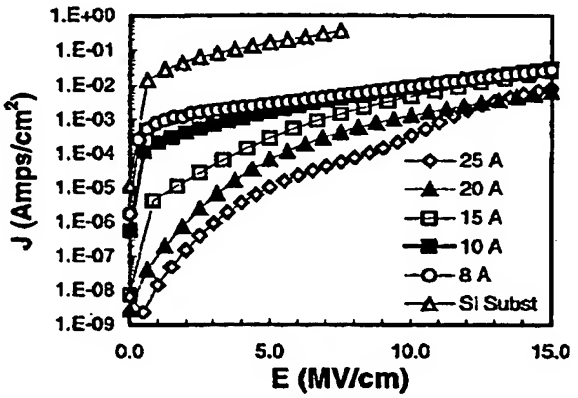

Fig. 1. Current density as a function of electric field for thin AlO_x films of various thicknesses deposited on bare Si substrates. As a comparison, the J–E characteristic of the bare Si substrate is also displayed.

The incorporation of the ALCVD reactor as a process module with a multichamber cluster tool ensures the process integrity and allows MTJ-typed metal/oxide multiplayer depositions. The metal layers NiFe, CoFe, Co, and IrMn were deposited using dc magnetron sputtering techniques in single-target physical vapor deposition modules.

Film magnetic properties were measured by an BH-looper (Shb Instruments, Inc.) and a vibration sample magnetometer (Digital Measurement Systems, Inc.). Film electric performance was evaluated by a CV probe (Four Dimension, Inc.), and MTJ device performance was characterized by a quasi-static tester.

III. Results and Discussion

High-quality ALCVD AlO_x films of amorphous nature were obtained with near-bulk properties and low pinhole density [2]. AlO_x films of thickness $\geq$ 50 Å show high breakdown strength over 9 MV/cm at a very low leakage current density of 7×10^{-6} Amps/cm^2. Typical leakage current density as a function of electric field is shown in Fig. 1 for ultrathin AlO_x films of thickness $\leq$ 25 Å deposited on bare Si substrates. It is clear that at these thicknesses the current leakage is dominated by direct electron tunneling. The current density-electric field (J–E) characteristics from the bare Si substrate clearly distinguish the contribution from the native SiO_2 from the overlaid AlO_x films.

The barrier height and thickness of these AlO_x films were estimated by current density versus voltage (J–V) characteristics. Typical J–V curves are plotted in Fig. 2. The data were fitted to the calculations from Simmons model [3], as shown by the solid line in the figure. The barrier height was determined to be (1.45 ± 0.05) eV for the three films and the barrier thickness to

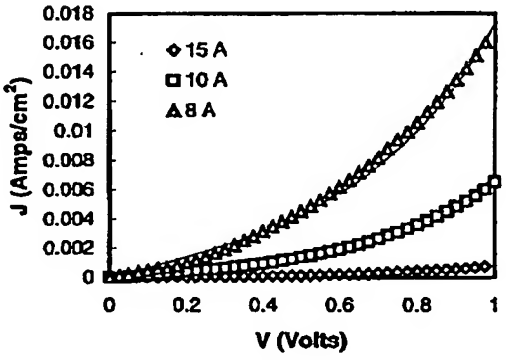

Fig. 2. Typical J–E characteristics of three thin AlO_x films. The solid lines represent the fit to the Simmons model.

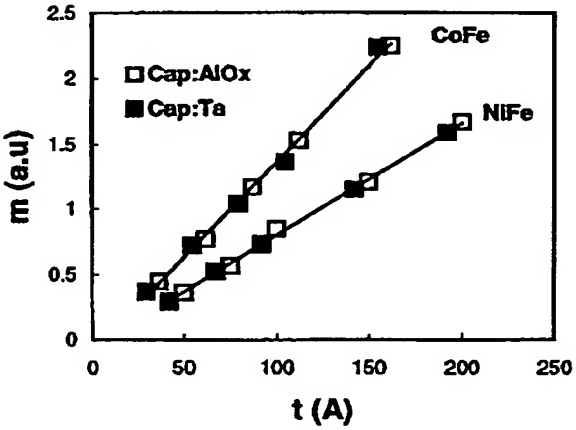

Fig. 3. Magnetic moment as a function of NiFe and CoFe layer thickness for a series films capped with an AlO_x 20-Å layer as opposed to a Ta50-Å layer. The data for the series with the Ta capping layer were intentionally shifted along the abscissa to compensate for the measured extra magnetic thickness loss.

be 12.4 ± 0.2, 13.2 ± 0.2, and 15.1 ± 0.1 Å, respectively, as compared with the nominal thickness of 8, 10, and 15 Å.

F r MTJ applications, care must be taken about the ALCVD process details to prevent the oxidation of the underlying magnetic layer upon exposure to H_2O. The process sequence was designed such that TMA was first delivered into the reactor to ensure one monolayer of TMA chemisorbed on the surface of the magnetic layer before introducing H_2O. The sequence was, therefore, $[TMA/Purge/H_2O/Purge]_n$ for n cycles of deposition. To confirm the validity of the process, a series of Ta50-Å/NiFe(t_{NiFe}) and Ta50 Å/NiFe20-Å/CoFe(t_{CoFe}) films were deposited capped with either an AlO_x20-Å layer r a Ta50-Å layer. The magnetic moment of these films was measured against the film thickness, as shown in Fig. 3. The moment-versus-thickness curves for the two series of films with AlO_x and Ta capping layers share the same slope, indicating equal magnetization value of these magnetic films. The data were fitted to a linear function. The intercept on the abscissa represents the magnetic thickness loss t_0. The results are summarized in Table I. Since these films were deposited on the same Ta50-Å underlayer, the difference in t_0 can be

TABLE I
MAGNETIC THICKNESS LOSS FOR NiFe AND CoFe FILMS WITH AN AlO_x 20-Å CAPPING LAYER OR A Ta50-Å CAPPING LAYER

Magnetic layer	NiFe	NiFe	CoFe	CoFe	NiFe[5]	CoFe[5]
Capping layer	AlO_x	Ta	AlO_x	Ta	Ta	Ta
t_0 (Å)	7.5	15.2	5.6	12.6	14.5	12.5

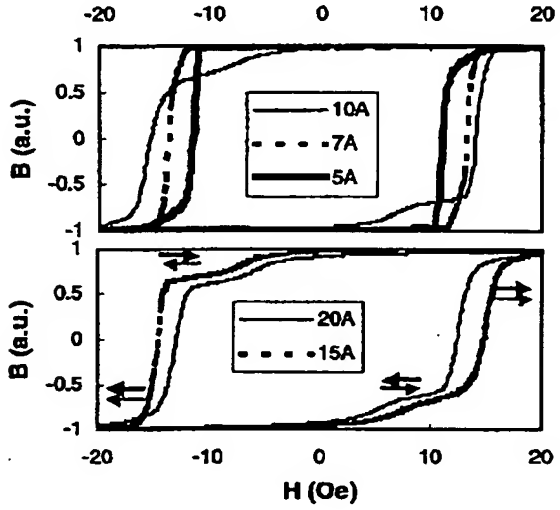

Fig. 4. Typical m-H loops manifest differential switching of the magnetizations for the two magnetic layers separated by an ultrathin AlO_x layer in Ta50-Å/NiFe50-Å/AlO_x(t_{AlO_x})-Å/NiFe50-Å/Co100-Å sandwich films, where t_{AlO_x} = 5, 7, 10, 15, 20 Å.

solely attributed to the difference in the capping layers. The intermixing and/or interdiffusion of Ta atoms into Co and NiFe films is well known [4], [5], and a 6.6-Å magnetic dead layer has been reported per Ta–Co interface in Ta–Co–Ta sandwich films [4]. This leads to an estimate of about 1 Å of magnetic dead layer at the NiFe–AlO_x and CoFe–AlO_x interfaces in the present case, which is much less than that with a Ta capping layer.

The decoupling of two magnetic layers sandwiching an AlO_x layer further tested the integrity of these ultrathin AlO_x layers. Differential switching of the magnetizations for the two magnetic layers with different coercivities was observed at a AlO_x spacer layer thicknesses $t_{AlO_x} > 7$ Å, as shown by the m-H loop in Fig. 4. The two-dimensional integrity of the ultrathin AlO_x layer is characterized by uniform thickness distribution and sharp interfaces with the two magnetic layers, which is distinctly illustrated by the transmission-electron-microscopy cross-sectional image from one of the sandwich films at t_{AlO_x} = 10 Å shown in Fig. 5.

Both the top and bottom IrMn exchange-biased MTJ films were deposited. As shown by the m-H loop in Fig. 6 for a CoFe100-Å/AlO_x14-Å/CoFe40-Å/IrMn150-Å film, the CoFe-free and pinned layers are clearly magnetically decoupled.

Magnetic tunnel junctions were fabricated with the junction areas from 0.01 mm^2 down to 10 μm^2 being defined by both shadow mask and optical lithography techniques. All the junctions tested so far have not shown any appreciable tunnel

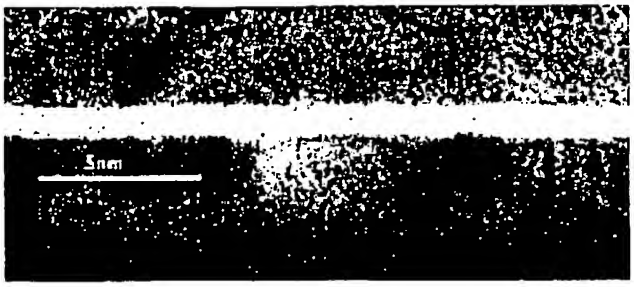

Fig. 5. Cross-sectional transmission-electron-microscopy image of a Ta50-Å/NiFe50 -Å/AlO_x 10-Å/NiFe50-Å/Co100-Å film.

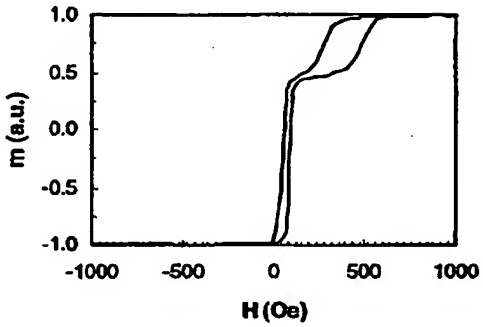

Fig. 6. Typical m-H loop for IrMn exchange-biased MTJ films are magnetically decoupled across the AlO_x barrier.

magnetoresistance. These junctions either show substantially low resistance values of a few ohms to a few thousand ohms with linear current–voltage (I–V) characteristics (junction #2 in Fig. 7), or high resistance values of a few million ohms with pronounced nonlinearity after a 30-s Ar:O_2 *in situ* plasma posttreatment [2] (junction #1 in Fig. 7).

The low junction resistance and the ohmic I–V feature indicate that the corresponding thin AlO_x barrier layers are Al-rich, deviating from the stoichiometric Al_2O_3. This is supported by the low values of measured barrier height 1.45 eV as compared with reported values $\geq$ 2 eV from naturally or plasma-oxidized thin AlO_x films. This can be attributed to the existence of a so-called incubation period in the early stage of the ALCVD process. The film thickness does not increase linearly with deposition cycles since the probability of the absorption of the reactants to a dissimilar surface other than AlO_x could be much lower. A proper *in situ* surface treatment may help uniform AlO_x nucleation on the underlying metallic magnetic layer without an incubation period. On the other hand, *in situ* Ar:O_2 plasma treatments at 150-mtorr and 100-W radio-frequency power level increased junction resistance substantially. The stoichiometric Al_2O_3 form could have been obtained for the

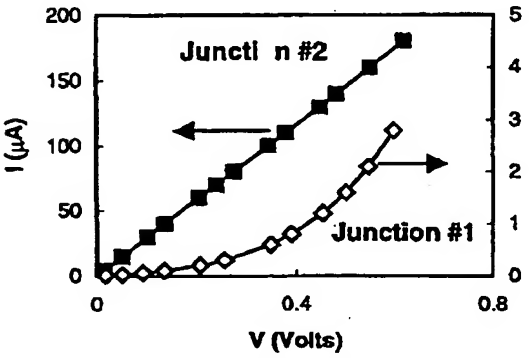

Fig. 7. I–V characteristics of two fabricated MTJ devices with a junction area of 10 10 μm^2 and a barrier thickness of 10 Å and 15 Å for junction #1 and #2, respectively.

thin barriers, however, at the expense of the partially damaged underlying CoFe layer due to the penetration of the energetic Ar or O ions that could extend over 20–30 Å at the bias voltage level applied ($\sim$ 100 V). A short duration with lower bias voltage level is recommended for further improvement.

Besides the aforementioned approaches, protecting the underlying magnetic layer can also make improvements. Deposition of a thin pure metal layer, such as Fe, as suggested in [6] or a thin layer of AlN *prior to* the AlO_x deposition will be effective.

IV. Conclusion

This is a brief evaluation of the ALCVD technology for MTJ barrier application. Although the outcome is not exciting, it has shed light on new directions. Future improvements will be focused on achieving ultrathin stoichiometric Al_2O_3 films and protecting the underlying magnetic layer from direct exposure to O_2-bearing precursors.

References

[1] T. Suntola, "Atomic layer epitaxy," *Thin Solid Films*, vol. 216, p. 84, 1992.
[2] A. Paranjpe, S. Gopinath, T. Omstead, and R. Bubber, "Atomic layer deposition of AlO_x for thin film head gap applications," *J. Electrochem. Soc.*, vol. 148, p. G465, 2001.
[3] J. G. Simmons, "Generalized formula for the electric tunnel effect between similar electrodes separated by a thin insulating film," *J. Appl. Phys.*, vol. 34, p. 1793, 1963.
[4] H. Lefakis, M. Benaissa, P. Humbert, V. S. Speriosu, J. Werckmann, and B. A. Gurney, "Structure and magnetism of Ta/Co/Ta sandwiches," *J. Magn. Magn. Mat.*, vol. 154, p. 17, 1996.
[5] C.-Y. Hung, M. Mao, S. Funada, T. Schneider, L. Miloslavsky, M. Miller, and H.-C. Tong, "Magnetic properties of ultra-thin NiFe and CoFe films," *J. Appl. Phys.*, vol. 87, p. 6618, 2000.
[6] Z. Zhang, S. Cardoso, P. P. Freitas, X. Batlle, P. Wei, N. Barradas, and J. C. Soares, "40% tunneling magnetoresistance after anneal at 380 °C for tunnel junctions with iron–oxide interface layers," *J. Appl. Phys.*, vol. 89, p. 6665, 2001.

Exhibit B

Available online at www.sciencedirect.com
SCIENCE DIRECT®
ELSEVIER
Journal of Magnetism and Magnetic Materials 262 (2003) 346–351
Journal of magnetism and magnetic materials
www.elsevier.com/locate/jmmm

A tunneling magnetoresistance sensor overlaid with a longitudinal bias stack

Tsann Lin*, Daniele Mauri, Philip M. Rice

IBM Almaden Research Center, San Jose, CA 95120, USA

Received 5 June 2002; received in revised form 4 November 2002

Abstract

In this study, a tunneling magnetoresistance (TMR) sensor overlaid with a longitudinal bias (LB) stack is fabricated, its magnetic and TMR properties are characterized, and its read performance is tested. The TMR sensor comprises Ta/Ni–Fe/Pt–Mn/Co–Fe/Ru/Co–Fe/Al–O/Co–Fe/Ni–Fe/Cu films, and the LB stack comprises Ru/Co–Fe/Pt–Mn/Ta films. A transverse-field anneal is applied to the TMR sensor to develop strong antiferromagnetic/ferromagnetic coupling within the Pt–Mn/Co–Fe films in a transverse direction perpendicular to an air bearing surface (ABS), thereby forming a transverse flux closure within the Co–Fe/Ru/Co–Fe films for operating the TMR sensor properly. A longitudinal-field anneal is applied to the LB stack to develop strong ferromagnetic/antiferromagnetic coupling within the Co–Fe/Pt–Mn films in a longitudinal direction parallel to the ABS, thereby forming a longitudinal flux closure within the Co–Fe/Ni–Fe/Cu/Ru/Co–Fe films for attaining stable TMR responses. The TMR sensor exhibits good magnetic and TMR properties, including low ferromagnetic coupling fields, high pinning fields, low junction resistance-area products, and high TMR coefficients. The TMR sensor overlaid with the LB stack shows stable, highly sensitive TMR responses.

Keywords: Magnetic recording; Tunneling magnetoresistance sensor; Ferromagnetic/antiferromagnetic coupling

1. Introduction

Various types of tunneling magnetoresistance (TMR) sensors have been extensively explored for magnetic recording at high areal densities ($\geqslant 10\,\mathrm{Gb/in^2}$) [1–3]. The most promising one of these TMR sensors, shown in Fig. 1, comprises Ta/Ni–Fe seed layers, a Pt–Mn transverse pinning layer, a Co–Fe keeper layer, a Ru spacer layer, a Co–Fe reference layer, an Al–O barrier layer, Co–Fe/Ni–Fe sense layers, and a Cu cap layer. To operate the TMR sensor properly, the magnetization of the keeper layer (M_3) must be rigidly pinned in a transverse direction perpendicular to an air bearing surface (ABS), the magnetization of the reference layer (M_2) must be rigidly pinned in an opposite direction, and the magnetization of the sense layers (M_1) is preferably oriented in a longitudinal direction parallel to the ABS. To attain stable TMR responses, the TMR sensor is proposed to be overlaid with a longitudinal bias (LB) stack [4]. The most promising LB stack, also shown in Fig. 1, comprises a Ru seed layer, a

*Corresponding author.
E-mail address: tsann@almaden.ibm.com (T. Lin).

0304-8853/03/$ - see front matter © 2003 Elsevier Science B.V. All rights reserved.
doi:10.1016/S0304-8853(02)01507-X

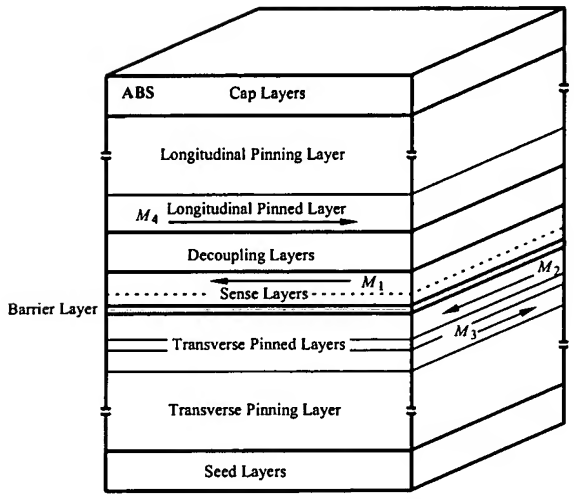

Fig. 1. Schematic of the structure of a TMR sensor overlaid with an LB stack.

Co–Fe longitudinal pinned layer, a Pt–Mn longitudinal pinning layer, and a Ta cap layer. The magnetization of the longitudinal pinned layer (M_4) must be rigidly pinned in a longitudinal direction parallel to the ABS in order to stabilize M_1 through magnetostatic interactions. This anitiferromagnetic (AFM) stabilization scheme differs from a conventional hard-magnetic (HM) stabilization scheme extensively used for a giant magnetoresistance (GMR) sensor, which is abutted with an LB stack comprising a Cr seed layer and an HM Co–Pt–Cr LB layer [5,6].

In order for the TMR sensor to perform magnetic recording at ultrahigh areal densities ($\geqslant$20 Gb/in^2), its thickness, width and height have been progressively reduced. The miniaturization of this TMR sensor causes substantial increases in demagnetization fields at sensor edges and more severe multidomain activities in the sense layers. It thus becomes more difficult to stabilize the sense layers. In this study, a TMR sensor overlaid with an LB stack is fabricated, its magnetic and TMR properties are characterized, and its read performance is tested.

2. Experimental

To evaluate a TMR sensor comprising Ta(6)/Ni–Fe(1)/Pt–Mn(20)/Co–Fe(1.6)/Ru(0.8)/Co–Fe(1.8)/Al–O(0.9)/Co–Fe(1)/Ni–Fe(1.6)/Cu(2)/Ta(6) films (thickness in nm), a bottom electrode comprising Al_2O_3(6)/Ta(6)/Cu(30) films and the TMR sensor were sequentially deposited on a Si substrate in an integrated ion-beam/DC-magnetron sputtering system. The Al–O film was formed by depositing an Al(0.6) film and in-situ oxidizing the Al film for 4 min in an oxygen gas of 2 Torr. After annealing the TMR sensor in a field of 10,000 Oe in the transverse direction for 5 h at 265°C, its magnetic properties were measured. After patterning the TMR sensor to a width of $\sim$1 μm and a height of $\sim$1 μm, its TMR properties were measured.

To evaluate the TMR sensor overlaid with an LB stack comprising Ru(1)/Co–Fe(2.8)/Pt–Mn(20)/Ta(15) films, the bottom electrode and the TMR sensor were sequentially deposited on a Si substrate in the integrated ion-beam/DC-magnetron sputtering system. After the transverse-field anneal, the oxidized Ta cap layer was removed, and then the LB stack was deposited and annealed together with the TMR sensor in a field of 100 Oe in the longitudinal direction for 5 h at 240°C. After this longitudinal-field anneal, its microstructure was observed with a transmission electron microscope (TEM). After patterning the TMR sensor overlaid with the LB stack to a width of $\sim$1 μm and a height of $\sim$1 μm, its read performance was tested.

The TMR sensor requires the transverse-field anneal to develop strong antiferromagnetic/ferromagnetic coupling between the Pt–Mn transverse pinning and Co–Fe keeper layers. The transverse field must exceed the saturation field (H_S) of ferromagnetic/ferromagnetic antiparallel (AP) coupling across the Ru spacer layer ($\sim$8000 Oe) for aligning M_3 and M_2 in the transverse direction. After cooling to room temperature, M_3 is rigidly pinned by the Pt–Mn transverse pinning layer in the transverse direction while M_2 is rotated by 180°. A transverse flux closure will be formed between M_3 and M_2 after patterning, resulting in a small net magnetization (M_2-M_3) in the Co–Fe/Ru/Co–Fe transverse pinned layers. This small net magnetization induces a small demagnetizing field in the sense layers, which balances with a ferromagnetic coupling field (H_F) across the Al–O

barrier layer. As a result, the sense layers are oriented in the longitudinal direction.

The LB stack requires the longitudinal-field anneal to develop strong ferromagnetic/antiferromagnetic coupling between the Co–Fe longitudinal pinned and Pt–Mn longitudinal pinning layers. The longitudinal field only needs to exceed the uniaxial anisotropy field (H_K) of the as-deposited Co–Fe longitudinal pinned layer ($\sim$20 Oe) for aligning M_4 in the longitudinal direction. After cooling to room temperature, M_4 is rigidly pinned by the Pt–Mn longitudinal pinning layer in the longitudinal direction. A longitudinal flux closure will be formed between M_4 and M_1 after patterning, inducing magnetostatic interactions needed for stabilizing the sense layers. Since this longitudinal field is much lower than the spin-flop field (H_{SF}) of ferromagnetic/ferromagnetic AP coupling across the Ru spacer layer ($\sim$1000 Oe), the transverse flux closure between M_3 and M_2 should not be interrupted.

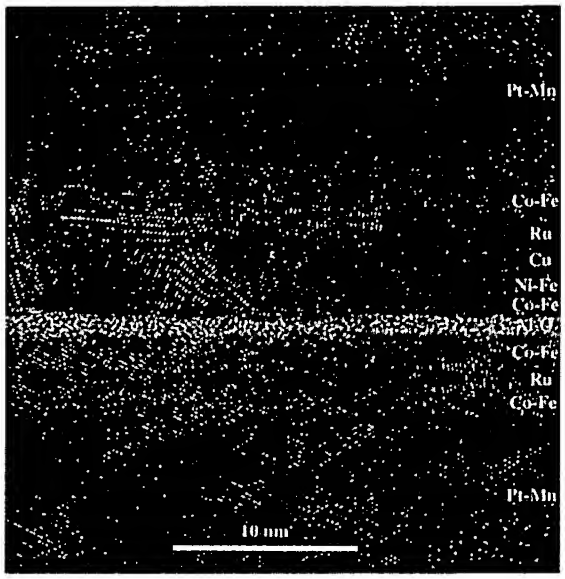

Fig. 2. A cross-sectional TEM micrograph of a TMR sensor overlaid with an LB stack.

3. Results and discussion

Fig. 2 shows a cross-sectional TEM micrograph of the TMR sensor overlaid with the LB stack. The Pt–Mn transverse pinning layer provides a smooth surface, which leads to the formation of flat Ru spacer and Al–O barrier layers. The Al–O barrier layer exhibits an entirely amorphous phase, without any remaining polycrystalline Al atoms. This amorphous phase stops the epitaxial growth of the underlying seed, transverse pinning and pinned layers, and facilitates the sense layers to grow freely.

Fig. 3 shows the areal moment (m) of the TMR sensor versus a magnetic field (H) applied in a direction parallel to the easy axis of the sense layers. The sense layers exhibit an areal moment (m_1) of 0.22 memu/cm^2, an easy-axis coercivity (H_{CE}) of 4.2 Oe, an H_K of 15.6 Oe, an H_F of 20.1 Oe, and a saturation magnetostriction (λ_S) of -0.5×10^{-6}. The transverse pinned layers exhibit a net areal moment ($m_2 - m_3$) of 0.04 memu/cm^2, an H_{SF} of 1,100 Oe, and an H_S of 8,000 Oe. These good magnetic properties indicate a potential use

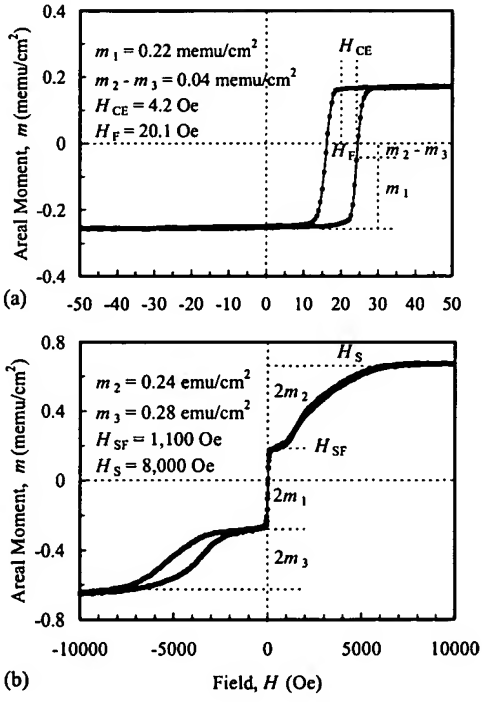

Fig. 3. m versus H for a TMR sensor.

of the TMR sensor for magnetic recording at ultrahigh areal densities.

Fig. 4 shows the TMR ratio of the TMR sensor ($\Delta R/R_J$) versus H, where R_J is a junction resistance measured when M_1, M_2 and M_3 are parallel to each other, and ΔR is a TMR. ΔR reaches a maximum value (ΔR_T) when M_1 is antiparallel to M_2. As shown in Fig. 4, the TMR coefficient of the TMR sensor ($\Delta R_T/R_J$) reaches as high as 19.0%. Fig. 5 shows $\Delta R_T/R_J$ versus a junction resistance-area product (R_JA_J). As R_JA_J increases from 4 to $10\,\Omega\,\mu m^2$, $\Delta R_T/R_J$ increases from 5% to 20%. The low R_JA_J is needed for minimizing electrostatic damages, while the high $\Delta R_T/R_J$ is needed for attaining high signal sensitivity.

The feasibility of the longitudinal-field anneal is evaluated by determining the rotation angle of the net magnetization of the transverse pinned layers (θ_2) after annealing a GMR sensor in a transverse field of 9000 Oe for 13.2 h at 260°C and then annealing it in a longitudinal field of 100 or 9000 Oe for various time (t_B) at various temperatures (T_B). The GMR sensor comprises multilayer

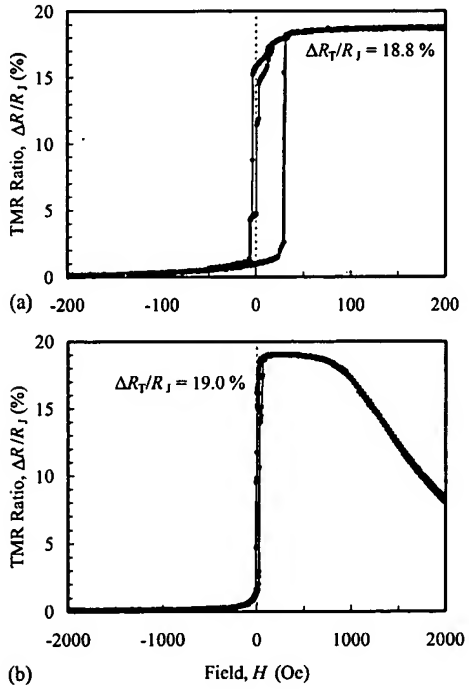

Fig. 4. $\Delta R/R_J$ versus H for a TMR sensor.

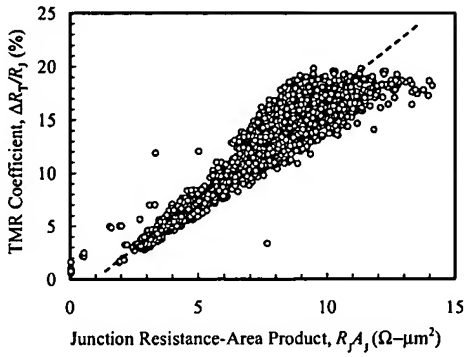

Fig. 5. $\Delta R_T/R_J$ versus R_JA_J for a TMR sensor.

films identical to those of the TMR sensor, except that the Al–O barrier layer is replaced by a Cu(2.1) spacer layer [7]. After cooling to 30°C in the field, θ_2 is determined from the asymmetry of hard-axis GMR responses [8]. The GMR sensor with transverse pinned layers identical to those of the TMR sensor is selected for the θ_2 determination, since patterning is not needed for measuring the GMR responses. Fig. 6 shows θ_2 as functions of t_B and T_B for the GMR sensor. After annealing in 100 Oe for 13.2 h at 220°C and 240°C, θ_2 is as small as 2° and 4.6°, respectively. However, after annealing in 9000 Oe for 13.2 h at 220 and 240°C, θ_2 is as large as 32.3° and 43.6°, respectively. These experimental results indicate that the longitudinal-field anneal in 100 Oe at 240°C can also be applied to the LB stack to develop the ferromagnetic/antiferromagnetic coupling, without substantially rotating the net magnetization of the transverse pinned layers from its preferred transverse direction.

The feasibility of the longitudinal-field anneal is also evaluated by determining H_{UA} of the LB stack after annealing the LB stack in a longitudinal field of 100 Oe for t_B at T_B. The LB stack comprises Al_2O_3(3)/Co–Fe(2.8)/Pt–Mn(20)/Ta(6) films. Fig. 7 shows H_{UA} as functions of t_B and T_B. H_{UA} increases from ~10 Oe to beyond 600 Oe after annealing for 2 h at 240°C or 260°C. In addition to the development of ferromagnetic/antiferromagnetic coupling for the LB stack, the longitudinal-field anneal also thermally resets M_1 to its preferred longitudinal direction. As a result, M_3 and M_2 stay in their preferred directions

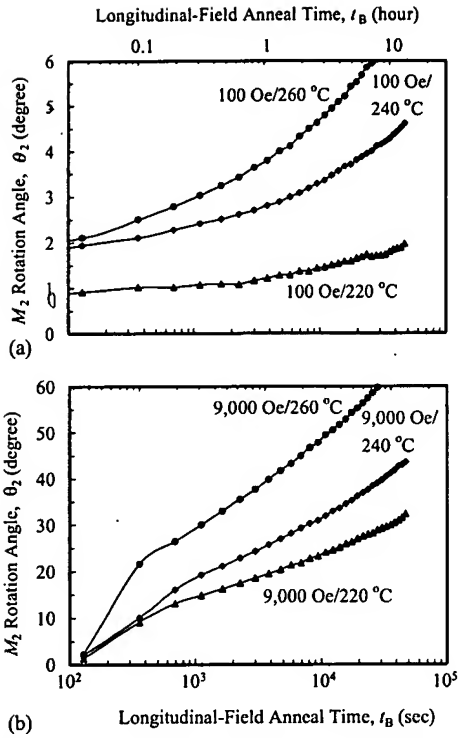

Fig. 6. θ_2 as functions of t_B and T_B for a GMR sensor after annealing in a transverse field of 9000 Oe for 13.2 h at 240°C and annealing in a longitudinal field of (a) 100 or (b) 9000 Oe.

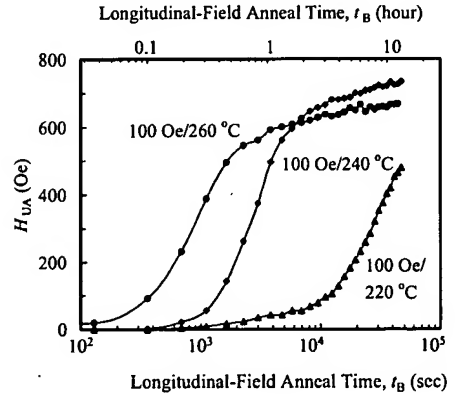

Fig. 7. H_{UA} as functions of t_B and of T_B for an LB stack after annealing in a longitudinal field of 100 Oe.

perpendicular to the ABS, while M_4 and M_1 stay in their preferred directions parallel to the ABS, without any thermal interruptions in the subsequent write head fabrication process.

The use of the LB stack has been found to substantially stabilize the sense layers. Fig. 8 shows TMR responses of the TMR sensor overlaid with the LB stack. As the thickness of the longitudinal pinned layer increases from 2.8 to 5.6 nm, its areal moment (m_4) increases from 0.36 to 0.72 memu/cm^2, while the H_{UA} of the LB stack decreases from 575 to 302 Oe. The TMR responses are stable and highly sensitive when m_4 is 0.36 memu/cm^2, but become less stable and less sensitive as m_4 increases. Hence, to stabilize the sense layers, an optimal m_4 and a high H_{UA} are needed in order to form a longitudinal flux closure and induce magnetostatic interactions between M_4 and M_1.

In this study, the AFM stabilization scheme is preferably used, since the TMR sensor and the LB stack are surrounded only by an insulating Al_2O_3 or SiO_2 film, and thus the sense current is confined to flow through the Al–O barrier layer for exhibiting TMR effects. In comparison with the HM stabilization scheme, the AFM stabilization scheme provides a better sensor-width control, higher read sensitivity, higher read efficiency, and more substantial side-reading suppression. The sensor-width control is better in the AFM stabilization scheme since the TMR sensor and the LB stack are confined only in the read region. The signal sensitivity is higher in the AFM stabilization scheme since an m_4 equivalent to $\sim$1.5 times m_1, instead of an areal remnant momant equivalent $\sim$6 times m_1 in the HM stabilization scheme, can be used to stabilize the

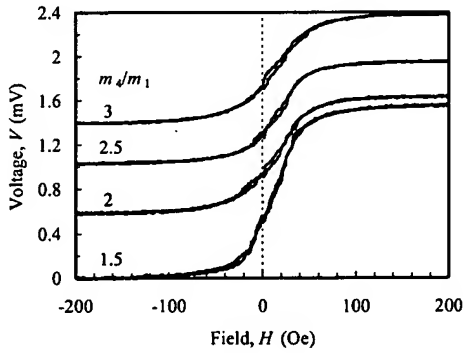

Fig. 8. TMR responses of a TMR sensor overlaid with an LB stack.

sense layers. The read efficiency is higher in the AFM stabilization scheme since the sensor edges are not interrupted by strong stray fields, which only stem from the Co–Pt–Cr LB layer in the HM stabilization scheme and induce sensor stiffness at the sensor edges. Side reading is more substantially suppressed in the AFM stabilization scheme since the sensor edges are abutted with the insulating Al_2O_3 or SiO_2 film, instead of the Co–Pt–Cr LB layer with complicated magnetics in the HM stabilization scheme. In spite of these advantages, the HM stabilization still receives extensive attentions due to its simplicity in orientating the remnant magnetization of the Co–Pt–Cr LB layer in the longitudinal direction at room temperature, and its extendibility into a TMR head with a much smaller read gap.

To ensure viability of the AFM stabilization scheme, it is crucial to ensure thermally stable antiferromagnetism of AFM films used as transverse and longitudinal pinning layers, and precisely control the total thickness of nonmagnetic films used as decoupling layers. In this study, the Pt–Mn films used as the transverse and longitudinal pinning layers require annealing to develop the needed antiferromagnetism, thus complicating the sensor fabrication process. Other AFM films which do not require annealing to develop the antiferromagnetism, such as Ir–Mn, Cr–Mn, etc., may be used to eliminate the longitudinal-field anneal. However, in general, these AFM films exhibit less thermally stable antiferromagnetism [9]. The nonmagnetic films used as decoupling layers comprise the Cu and Ru films. The Cu film also acts as a cap layer for in situ protecting the sense layers, while the Ru film also acts as a seed layer for facilitating the longitudinal pinned and pinning layers to attain a high H_{UA}. Their total thickness should be optimized in order to diminish ferromagnetic/antiferromagnetic coupling between the longitudinal pinned and sense layers, while still ensuring strong magnetostatic interactions between the longitudinal pinned and sense layers. It is difficult to precisely control this total thickness due to the use of the sacrificial Ta cap layer for protecting the TMR sensor during the transverse-field anneal. Hence, the sensor fabrication process described in this study needs further improvements.

5. Conclusions

A TMR sensor overlaid with an LB stack has been fabricated, its magnetic and TMR properties have been characterized, and its read performance has been tested. A transverse-field anneal has been applied to the TMR sensor for operating the TMR sensor properly, and a longitudinal-field anneal has been applied to the LB stack for stabilizing the sense layers. The TMR sensor can be operated properly due to the formation of a transverse flux closure within the transverse pinned layers, and the sense layers can be stabilized due to the formation of a longitudinal flux closure within the longitudinal pinned and sense layers. The TMR sensor has been found to exhibit good magnetic and TMR properties, and its TMR responses have been found to be stable and highly sensitive. The TMR sensor overlaid with the LB stack is thus expected to be viable for magnetic recording at ultrahigh areal densities.

References

[1] J.S. Moodera, L.R. Kinder, T.M. Wong, R. Meservey, Phys. Rev. Lett. 74 (1995) 3273.
[2] T. Miyazaki, N. Tezuka, J. Magn. Magn. Mater. 139 (1995) L231.
[3] K. Ohashi, K. Hayashi, K. Nagahara, K. Ishihara, E. Fukami, J. Fujikata, S. Mori, M. Nakada, T. Mitsuzuka, K. Matsuda, H. Mori, A. Kamijo, H. Tsuge, IEEE Trans. Magn. 36 (2000) 2549.
[4] F.H. Dill, R.E. Fontana, T. Lin, S.S.P. Parkin, C.H. Tsang, US Patent, 6,023,395, February 8, 2000.
[5] H. Ueno, K. Nishida, F. Mizukami, K. Hikami, T. Tabuchi, Sawasaki, IEEE Trans. Magn. 36 (2000) 2572.
[6] N. Hasegawa, M. Saito, K. Tanaka, Y. Ide, F. Koike, Y. Nakazawa, T. Kuriyama, Magn. Soc. Jpn. 24 (2000) 1239.
[7] T. Lin, D. Mauri, Appl. Phys. Lett. 78 (2001) 2181.
[8] T. Lin, D. Mauri, IEEE Trans. Magn. 35 (1999) 2607.
[9] T. Lin, C. Tsang, J. Magn. Soc. Jpn. 22 (S1) (1998) 103.